



HAL
open science

Specularity removal: a global energy minimization approach based on polarization imaging

Fan Wang, Samia Ainouz, Caroline Petitjean, Abdelaziz Bensrhair

► To cite this version:

Fan Wang, Samia Ainouz, Caroline Petitjean, Abdelaziz Bensrhair. Specularity removal: a global energy minimization approach based on polarization imaging. *Computer Vision and Image Understanding*, Elsevier, 2017. hal-02114528

HAL Id: hal-02114528

<https://hal-normandie-univ.archives-ouvertes.fr/hal-02114528>

Submitted on 29 Apr 2019

HAL is a multi-disciplinary open access archive for the deposit and dissemination of scientific research documents, whether they are published or not. The documents may come from teaching and research institutions in France or abroad, or from public or private research centers.

L'archive ouverte pluridisciplinaire **HAL**, est destinée au dépôt et à la diffusion de documents scientifiques de niveau recherche, publiés ou non, émanant des établissements d'enseignement et de recherche français ou étrangers, des laboratoires publics ou privés.

Specularity removal: a global energy minimization approach based on polarization imaging

Fan Wang^{a,b,*}, Samia Ainouz^b, Caroline Petitjean^b, Abdelaziz Bensrhair^b

^a*Research Institute of Intelligent Control & Image Engineering, Xidian University, 710071, Xi'an, China*

^b*LITIS laboratory, INSA de Rouen, 76801, Saint-Etienne du Rouvray, France*

Abstract

Concentration of light energy in images causes strong highlights (specular reflection), and challenges the robustness of a large variety of vision algorithms, such as feature extraction and object detection. Many algorithms indeed assume perfect diffuse surfaces and ignore the specular reflections; specularity removal may thus be a preprocessing step to improve the accuracy of such algorithms. Regarding specularity removal, traditional color-based methods generate severe color distortions and local patch-based algorithms do not integrate long range information, which may result in artifacts. In this paper, we present a new image specularity removal method which is based on polarization imaging through global energy minimization. Polarization images provide complementary information and reduce color distortions. By minimizing a global energy function, our algorithm properly takes into account the long range cue and produces accurate and stable results. Compared to other polarization-based methods of the literature, our method obtains encouraging results, both in terms of accuracy and robustness.

Keywords: specularity removal, polarization, diffuse, separation, energy minimization

*corresponding author

Email address: fan.wang@insa-rouen.fr (Fan Wang)

1. Introduction

Based on the dichromatic reflection model [1], each brightness value in an image is viewed as the sum of two components, the diffuse and the specular parts. Most opaque surfaces have a combination of specular and diffuse elements due to surface structure. The diffuse element is viewable from all directions while the specular part behaves based on Snells law [2], so is only visible when viewed from the correct orientation. The specular reflection appears to be a compact lobe on the object surface around the specular direction, even for rough surfaces [3]. Whereas the diffuse component represents the actual appearance of an object surface, specularity reflection is an unwanted artifact that can hamper high-level processing tasks such as visual recognition, tracking, stereo reconstruction, objects re-illumination [4, 5]. Specularity removal, a challenging topic in computer vision, is thus a decisive preprocessing for many applications [6].

1.1. Related works

The light reflection always carries important information of a scene, so that the separation of the reflection gives a way to better analyze the scene. Nayar et al. [7] separates the reflection using structured light, which conveys useful properties of the object material as well as the media of the scene. O’Toole et al. [8] also use structured light in reflection separation to recover the 3D shape of the object. While the above methods have shown good performance in their applications, they analyze the scene through the direct and global reflection components, whereas we analyze it through the specular and diffuse reflections. Direct components contain both specular and diffuse reflections, while global components arise from interreflections as well as from volumetric and subsurface scattering. The direct/global separation handles complex reflections, which may result in useful material related information ; however it requires strict controllable light source, which limits this usability of this separation. On the other hand the specular/diffuse component analysis deals with

30 natural light source, which makes it more valuable. The separation of specular/diffuse components is thus regarded as pre-processing step, since specular reflection might be problematic in several computer vision tasks, such as stereo matching, image segmentation or object detection.

There are also works that aim at separating the diffuse and specular components under polarized light source. For instance, in [9] a robust diffuse/specular reflection separation method is proposed, but is designed to only work for scene under controllable light source. In this work, we take a different approach leading to a generalization of the applicability: we deal with scenes under uncontrollable light source, in order to imitate outdoor illumination conditions.

40 Traditional methods separate the diffuse and specular components using color-only images, based on the idea to find a variable which is independent from the specular component. By estimating this variable for each given pixel, the diffuse component may be computed. As a seminal work in color-based methods, Tan et al. [10] inspects the specular component via chromaticity, which is proved to be independent from the specular component. An additional hue-based segmentation method is required for the multi-colored surfaces. Yang et al. [11] extend this work by detecting diffuse pixels in the HSI space, which also requires hue-based segmentation. The color covariance is defined as a constant variable to recover the diffuse component. Kim et al. [12] use the dark channel prior as a pseudo-solution and refine the result through the Maximum A Posteriori (MAP) estimation of the diffuse component. The dark channel prior, however, only works for highly colored surfaces. To avoid extra segmentation, Tan and Ikeuchi [13] propose another diffuse pixel pick-up method via computing the logarithmic differential between up to four neighboring pixels. 50 The common limitation of the above presented color-based methods is their high color distortion on the recovered diffuse component [13, 3, 11]. The main reason is that these methods assume that the specular color is constant throughout the image.

To better recover the diffuse component, other methods proposed to accomplish the separation using polarization images [14], since specular and diffuse 60

components hold different degrees of polarization (DOP). The DOP represents the ratio of the light being polarized. When a beam of unpolarized light is reflected, the DOP of specular reflection is larger than that of the diffuse reflection for most angles of incidence, meaning that the specular reflection is generally
65 much more polarized than the diffuse reflection [15]. When rotating the polarizer, the change of the intensity is only related to the specular part, so that the intensity change refers directly to the specular color.

With these constraints, polarization based methods produce more accurate results with less color distortions. The pioneering work of Nayar et al. [3]
70 constrains the diffuse color on a line in RGB space. The neighboring diffuse-only pixels are used to estimate the diffuse component, providing state-of-the-art polarization-based specular removal results. However, specular pixels are detected by simple thresholding of the DOP. The DOP changes not only with different specular portions, but also with different incident angles and different
75 indices of refraction. The computation of the DOP involves more than three images, making it largely contaminated by camera noise. This makes Nayar’s method prone to error since its computation highly relies on the DOP.

The methods presented above are local and based on the dichromatic reflection model [1]. These methods assume that the intensity of a pixel is a
80 linear combination of its diffuse and specular components. On the other hand, a global-based method presented in [16] simplifies this model into the image level, under the conditions that the light source is far away from the object and that the incident angle does not change. In other words, the acquired image is linearly combined by a specular image and a diffuse image with respect to a
85 constant parameter. This parameter is reversed using the Independent Component Analysis (ICA) [17]. However, these ideal conditions discussed in [16] rarely conform to reality, thus only a part of the specular reflection component is removed.

With respect to the literature, we make the following observations: (i) color-
90 based methods produce heavy color distortions; (ii) local patch-based methods can only use the information offered by neighboring pixels without any consid-

eration of long range cues. Based on these observations, we proposed in this article a global method using the polarization setup and a local approximate solution as detailed in the next subsection.

95 *1.2. Contribution*

Our approach builds upon Umeyama’s method [16] and share conceptual similarities. However, we propose a threefold contribution : (i) As in [16] we assume that the acquired image is the linear combination of a diffuse and specular reflection images. However, we depart from the use of a fixed weighting coefficient and instead investigate the benefit of using a spatially varying coefficient, which generalizes the model proposed in [16] to better conform to the reality. The use of the spatially varying parameter additionally enables the algorithm to work with scenes under (non-overlapping) multi-sources of illumination. (ii) Based on these assumptions, a global energy function is constructed to leverage long range information, that patch based method cannot handle, by construction. In patch based methods, the solution for one pixel is influenced only by the local neighborhood. In a graph based approach, pixels are connected through the graph construction, and their interdependency is accounted thanks to the smoothness term; additionally, the graph energy is minimized globally. The expectation is that by optimizing the problem globally, results will be more accurate and robust than with local patch-based methods. The optimum solution is found by applying the graph cuts algorithm [18]. (iii) Apart from the independence assumption, a first approximate solution is computed as a supplementary constraint. We propose to compute a more reliable approximate solution by combining the specular detection method in [13] and the specularity reduction in [3]. Lastly, in the experimental part, a histogram-based criterion is proposed to quantitatively evaluate the results. The proposed method is compared with two well-known separation algorithms : Nayar’s polarization setup [3] and Umeyama’s method [16]. This paper extends upon our previous preliminary work [19] in the following aspects. In the current paper, we fully elaborate on the idea and the steps of the computation of the first approximate

100
105
110
115
120

solution. The computation of the data term is accurately described, as well as the smoothness term, and the justification as to why the solution is ensured to be stable. This paper contains some additional illustration to demonstrate
 125 more clearly the improvement of the proposed global method. Supplementary experiments are also reported, including the study of the algorithm robustness in the presence of noise.

1.3. Overview

In the remainder of the paper, we first present our polarization system in
 130 Section 2. The problem formulation is defined in Section 3. In section 4, we describe the proposed global energy function, and explain each term in detail. In Section 5, we describe the implementation of the method with a discussion about the results. Finally, we offer some perspectives to this work in Section 6.

2. Polarization system

135 The light reflection from an object is a combination of diffuse and specular components, in which the specular component is generally partially linearly polarized. It is fully described by three parameters [20]: light magnitude I , degree of polarization ρ , angle of polarization φ . In order to measure the polarization parameters, a polarizer rotated by an angle α is installed in front of the camera
 140 as shown in Fig. 1 (a). Several images $I_p(\alpha_i)$ are acquired by rotating the polarizer to different positions α_i . The intensity $I_p(\alpha_i)$ of each pixel is linked to the polarizer angle α_i and the polarization parameters by the following equation:

$$I_p(\alpha_i) = \frac{I}{2}[\rho \cos(2\alpha_i - 2\varphi) + 1] \quad (1)$$

Since there are three unknown parameters (I , ρ and φ) to be determined in Equation (1), at least three images need to be acquired with different α_i . Fig.
 145 1 (b) shows the variation curve of $I(\alpha_i)$, where for each pixel, I_{max} and I_{min} refer to the maximum and minimum intensity, respectively.

Regarding the number of images to be acquired, different configurations are possible, such as 36 images in [21]. The more images are acquired, the

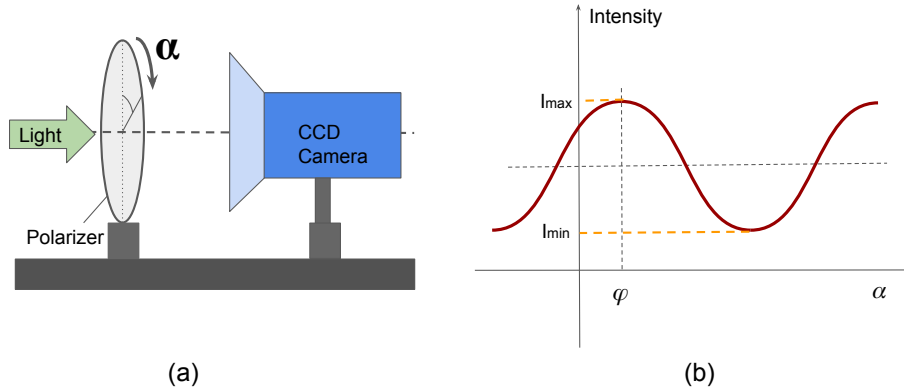


Figure 1: (a) Polarization imaging system; (b) Variation of intensity by rotating the polarizer angle α .

more stable the results will be. However, in this paper, we chose to use three
 150 images since current hardware capture no more than three polarization images
 simultaneously [22], and since we aim at solving this problem for potentially
 real-time applications.

Once all three parameters have been estimated, I_{max} and I_{min} can be com-
 puted thanks to:

$$I = I_{max} + I_{min}, \quad \rho = \frac{I_{max} - I_{min}}{I_{max} + I_{min}} \quad (2)$$

155 3. Problem formulation

From the dichromatic reflectance model [23], a beam of light is a linear
 combination of the diffuse and specular components. Umeyama et al. [16] have
 simplified this model to the image level by assuming that the acquired image I
 is the sum of a diffuse image I_d and a specular image I_s , where the I_s is a raw
 160 specular image \mathring{I}_s combined with a fixed weighting coefficient p as shown in Fig.
 2 (a). The image I is thus related to its components according to:

$$\begin{cases} I(x) = I_d(x) + I_s(x) \\ I_s(x) = p\mathring{I}_s(x) \end{cases} \quad (3)$$

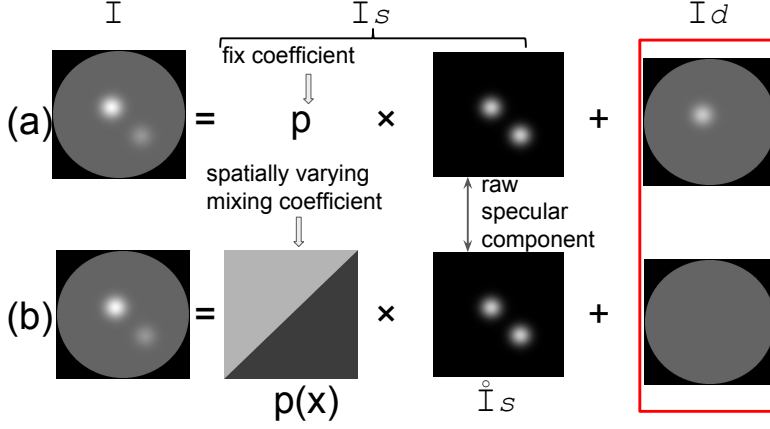


Figure 2: Modeling an image I as a linear combination of a diffuse component I_d and a raw specular component I_s , with (a) a fixed coefficient as in Umeyama et al. [16], it can be seen that the specular component is not fully removed from I_d ; (b) a spatially varying coefficient as assumed in our approach, which more effectively removes the specular reflection.

The raw specular image $\overset{\circ}{I}_s$ is defined as:

$$\overset{\circ}{I}_s = I_{max} - I_{min} \quad (4)$$

where I_{max} and I_{min} are the maximum and minimum intensity described in Equation (2). The goal is to estimate p , as then the corresponding diffuse $I_d(x)$ and specular components $I_s(x)$ can be computed using Equation (5). The diffuse and specular reflection images being assumed probabilistically independent, the optimum p can be found by minimizing the Mutual Information (MI) [24, 16] between I_d and I_s to ensure their maximum independence.

This method globally models the diffuse and specular separation problem, however it suffers from some limitations. First, in real applications, the assumption that the incident angle on each pixel remains constant is not always valid. Hence, setting a single value for the weighting coefficient over the whole image is inconsistent. As a consequence, the computation of MI, which is computa-

tionally costly, becomes unfeasible or at least unrealistic¹, since the sum of MI
 175 needs to be minimized at each local patch.

We propose to tackle these limitations through the following improvements:
 (i) The mixing coefficient is assumed to be spatially varying as shown in Fig.
 2(b). As one can see, the specular reflection is more effectively removed from
 the computed diffuse component in Fig. 2(b) than in Fig. 2(a); (ii) As in
 180 [16] We assume that I_d and I_s are probabilistically independent. The goal is
 to minimize their similarity. Since only maximizing the independence is not
 enough to produce the best solution, we introduce a first approximate solution
 as a constraint to ensure the reliability of the final solution; (iii) Instead of MI,
 we propose to compute another more efficient similarity measurement which
 185 produces competitive results.

4. Global energy function

As global methods can better integrate the long range cue via the global
 smoothness assumption, they can produce more accurate and robust result than
 local patch-based methods. For this purpose, we propose a global energy func-
 190 tion, which is composed of a data term and a smoothness term.

As mentioned above, in this paper we assume that the mixing coefficient is
 spatially varying. Equation (3) is transformed into:

$$\begin{cases} I(x) = I_d(x) + I_s(x) \\ I_s(x) = p(x)\hat{I}_s(x) \end{cases} \quad (5)$$

where the $p(x)$ is the local weighting coefficient.

From Umeyama et al. [16], the specular component $p(x)\hat{I}_s(x)$ is decided by
 195 the surface geometry and the angle of incidence of the light which is generally
 locally smooth. As $\hat{I}_s(x)$ represents the unit color vector of pixel x , we make
 a smooth assumption on the term $p(x)$, which enforces the continuity of the

¹on a laptop running with a 2.6 GHz processor and 8GB RAM.for about 25 minutes for a
 240 × 320 image.

specular component. To consider the sharp change that might originate from the different structures of the scene, we have included a color discontinuity
 200 detection method in Section 4.2. Our objective is to find an optimum $p(x)$ for each pixel x .

Let $\Phi(p(x))$ denote the data term and $\Psi(p(x), p(y))$ the smoothness term of the global energy function. The optimum $p(x)$ can be found by solving the following constraint optimization problem:

$$\begin{aligned} \operatorname{argmin}_{p(x)} \left[\sum_x \Phi(p(x)) + \lambda_1 \sum_x \sum_{y \in \mathcal{N}(x)} \Psi(p(x), p(y)) \right] \\ \text{s.t. } 0 \leq p \leq \tilde{p} \end{aligned} \quad (6)$$

205 where $y \in \mathcal{N}(x)$, $\mathcal{N}(x)$ refers to the 4-connected neighborhood of x , λ_1 is a hyper-parameter which balances the data and the smoothness terms. While solving the minimization problem, a large p value may result in a negative intensity of I_d (from Equation (5)). For this reason, pixel-wise dependent scalar \tilde{p} is applied on p as an upper bound, so that I_d is always kept positive.

210 4.1. Minimization algorithm: graph cuts

This energy function in Equation (6) is solved by using the graph-cut algorithm. The image is considered as a graph: each pixel is represented by a node, and the edge weights between nodes are related to the similarity between the nodes (smoothness term in Eq (6)). Each node is also linked so special nodes
 215 which express the constraint given by the problem knowledge, i.e. the data term in Eq (6). A graph cut is a partition of the graph (i.e. the image). Each possible partition has a cost, which can be expressed as the sum of the weights of the edges cut when partitioning. The optimum segmentation is the lowest-cost cut in the graph, and it can be efficiently solved using the α -expansion [18], an
 220 algorithm well-known for its effectiveness in solving large global optimization problems [25].

4.2. Data term

The data term $\Phi(p(x))$ contains two parts: a patch-based dissimilarity (independence) measurement $C_{DC}(p(x))$, and a pixel-wise constraint $D(p(x))$:

$$\Phi(p(x)) = -\lambda_2 C_{DC}(p(x)) + D(p(x)) \quad (7)$$

where λ_2 is a weighting hyper-parameter. The term $C_{DC}(p(x))$ is used to maximize the independence between the diffuse and the specular images. However, using this term only tends to over-smooth the solution, leading us to introduce an additional constraint in this data term, denoted $D(p(x))$. This constraint is based on an initial approximate solution and enforces the similarity between the final solution and this initial result. Using an initial solution has several advantages: first, it ensures the reliability of the result. In addition, the first solution used as the initialization to the optimization process also improves the time efficiency. By minimizing $\Phi(p(x))$, the optimum $p(x)$ is found through the trade-off between maximizing $C_{DC}(p(x))$ and minimizing $D(p(x))$.

4.2.1. Dissimilarity measurement

Dissimilarity between diffuse and specular images is usually measured through mutual information [16]. Since using mutual information for a patch centered at each pixel is highly time consuming, we take advantage of another criterion, which from our experiments, yields similar results as compared to mutual information and is less time consuming. This criterion, called *DIFFcensus* [26] has been shown to be an efficient criterion to optimize the disparity map. It is known to be resistant to noises and color distortions.

Let us now define the *DIFFcensus* cost function. Given a pixel location x and an arbitrary $p(x)$ ($0 \leq p(x) \leq \tilde{p}(x)$), the independence between the diffuse component $I_d(x)$ and its corresponding specular component $I_s(x)$ is measured with:

$$\begin{aligned} C_{DC}(p(x)) &= \text{DIFFcensus}(I_d(x), I_s(x)) \\ &= g(C_{census}(\bar{I}_d(x), \bar{I}_s(x)), \lambda_{census}) \\ &+ g(C_{DIFF}(\bar{I}_d(x), \bar{I}_s(x)), \lambda_{DIFF}) \end{aligned} \quad (8)$$

where $g(C, \lambda) = 1 - \exp(-\frac{C}{\lambda})$, and $\bar{I}_d(x)$ and $\bar{I}_s(x)$ are $n \times m$ patches centered at x with arbitrary size ($n = m = 5$ in our experiments). λ_{DIFF} and λ_{census} are hyperparameters balancing the two parts, set to default values $\lambda_{DIFF} = 55$ and $\lambda_{census} = 95$ as suggested in [26]. More specifically, in Equation (8), we have:

$$\begin{cases} C_{census}(\bar{I}_d(x), \bar{I}_s(x)) = H(CT(\bar{I}_d(x)), CT(\bar{I}_s(x))) \\ C_{DIFF}(\bar{I}_d(x), \bar{I}_s(x)) = \frac{|DIFF(\bar{I}_d(x)) - DIFF(\bar{I}_s(x))|}{n \times m} \end{cases} \quad (9)$$

where $CT(\cdot)$ refers to the Census Transform, and $H(\cdot)$ is the Hamming distance. For more information about CT and Hamming distance, please refer to [27]. $DIFF(\cdot)$ is computed as:

$$\begin{cases} DIFF(\bar{I}_d(x)) = \sum_{y \in \bar{I}_d(x)} |I_d(x) - I_d(y)| \\ DIFF(\bar{I}_s(x)) = \sum_{y \in \bar{I}_s(x)} |I_s(x) - I_s(y)| \end{cases} \quad (10)$$

The $DIFF_{census}$ function represents a trade-off between the classical CT and the Sum of Absolute Difference which are balanced via hyperparameters λ_{DIFF} and λ_{census} . Results are improved compared to using these criteria alone [26].

4.2.2. Constraint term

The independence assumption alone does not provide a good separation result. In order to guide the separation process, we introduce a constraint on the final solution $p(x)$ to enforce its similarity to a first approximate solution $p_{init}(x)$. The constraint term is given by measuring:

$$D(p(x)) = |p(x) - p_{init}(x)| \quad (11)$$

The first approximate solution $p_{init}(x)$ is found by combining the logarithm differential specular detection method proposed by [13] and the specular-to-diffuse mechanism in [3]. The computation of $p_{init}(x)$ is detailed in Section 4.4.

4.2.3. Stability of the solution

The aim of the data term is to find $p(x)$ that numerically minimizes $\Phi(p(x))$. The problem is to find a trade-off between maximizing C_{DC} and minimizing $D(p(x))$ so that the final solution does not go randomly far from an approximate solution p_{init} . The minimum of this functional cannot degenerate to infinity because our space is of finite dimension (pixels) and the functional $\Phi(p(x))$ is continuous and bounded from below. Let us demonstrate these points. By construction, the research space of the solution $p(x)$ is in the domain $[0, \tilde{p}(x)]$ ($0 \leq p(x) \leq \tilde{p}(x)$) where $\tilde{p}(x) \in [0, 255]$ is an upper bound so that the diffuse image I_d is always positive. The minimum of the functional $\Phi(p(x))$ is searched within this domain.

Regarding the C_{DC} term, from the Equation (8), it is a combination of two functions g , where $g(x) = 1 - \exp(-x)$ and is bounded by 1. Thus

$$C_{DC}(p(x)) = g(C_{census}, \lambda_{census}) + g(C_{Diff}, \lambda_{Diff}) < 2 \quad (12)$$

Regarding the $D(p(x))$ term, it is the absolute value of the difference between $p(x)$ and the first approximate solution p_{init} . $D(p(x))$ is thus positive and finite also because $0 \leq p(x) \leq \tilde{p}(x)$.

Consequently, $\Phi(p(x))$ has a lower bound, ensuring the stability of the solution:

$$\Phi(p(x)) = -\lambda_2 C_{DC}(p(x)) + D(p(x)) > -2\lambda_2 \quad (13)$$

4.3. Smoothness term

The smoothness term is classically computed among the 4-connected neighborhood $\mathcal{N}(x)$ of the pixel x . To better take into account the original texture of the image, we implement a color discontinuity detection based on thresholding RGB values, as suggested in [13]. Let ThR and ThG be small threshold values (one should adjust this value according to the input images, here default values $ThR = ThG = 0.005$ as in [13] are used in this paper), and indices r and g be the red and green channels in the RGB space. A color discontinuity on the pixel

x is defined as follows:

$$(\delta_r(x) > ThR \text{ and } \delta_g(x) > ThG) \begin{cases} \text{true: color discontinuity} \\ \text{false: no color discontinuity} \end{cases} \quad (14)$$

where

$$\begin{cases} \delta_r(x) = \sigma_r(x) - \sigma_r(x-1) \\ \delta_g(x) = \sigma_g(x) - \sigma_g(x-1) \end{cases} \quad (15)$$

295 and

$$\begin{cases} \sigma_r = \frac{I_r}{I_r + I_g + I_b} \\ \sigma_g = \frac{I_g}{I_r + I_g + I_b} \end{cases} \quad (16)$$

Chromaticity changes are computed between neighboring pixels on both red and green channels (the blue channel is not included since $\sigma_r + \sigma_g + \sigma_b = 1$). This method detects the color discontinuity, which helps to maintain the original texture of the object, as well as to prevent the smoothness term from running
300 over the object boundary (where the sharp change of the object shape appears).

The smoothness term is defined as:

$$\Psi(p(x), p(y)) = \begin{cases} 0, & \text{if } x \text{ is located on a color discontinuity} \\ \sqrt{p(x)^2 - p(y)^2} & \text{otherwise} \end{cases} \quad (17)$$

4.4. First approximate solution

The first approximate solution $p_{init}(x)$ provides an additional constraint to the data term to improve the accuracy of the model, as well as a sub-optimal
305 initial solution to improve the efficiency of the subsequent optimal process.

To locally obtain an approximate solution, we propose two steps: specular region detection and specularity reduction. For specularity detection, polarization-based methods usually apply a simple thresholding on the DOP as in [3], which is unreliable because of noise. Also the threshold largely varies
310 from scene to scene. Thus we will rely upon Tan's approach [13]. For specular removal, however, we did not follow Tan for specular reduction, since for

RGB, there is no color constraint whereas there is one for polarization images. Tan’s method does not fully make use of the richness of polarization images. For this reason, we propose Nayar’s approach [3]. In the following, we describe
 315 each step of specularity detection and reduction and how we propose to combine them sequentially.

4.4.1. Specularity detection

For RGB images, Tan notices in [13] that making the pixel saturation constant with regard to the maximum chromaticity while retaining their hue, allows
 320 to successfully remove highlights. The chromaticity is defined as the normalized RGB:

$$\Lambda(x) = \frac{I(x)}{I_r(x) + I_g(x) + I_b(x)} \quad (18)$$

where $\Lambda = \{\Lambda_r, \Lambda_g, \Lambda_b\}$. The maximum chromaticity is defined as :

$$\tilde{\Lambda}(x) = \frac{\max(I_r(x), I_g(x), I_b(x))}{I_r(x) + I_g(x) + I_b(x)} \quad (19)$$

For the whole image, the $I(x)$ is shifted so that the maximum chromaticity $\tilde{\Lambda}(x)$ is turned to an arbitrary constant value (we set $\tilde{\Lambda}(x) = 0.5$ as suggested
 325 by [13]), yielding a new image I' , where highlights are removed. However this method yields color distortions in I' and is limited to weak specular highlights. Thus, a logarithm differential step is added. Let y be a neighboring pixel of x , the logarithm differential $\delta(x, y)$ is computed as:

$$\delta(x, y) = \log \frac{I(x)}{I(y)} - \log \frac{I'(x)}{I'(y)} \quad (20)$$

Tan shows indeed that if two neighboring pixels are both diffuse pixels, their
 330 intensity logarithm differential is zero, meaning that their log ratio still keeps the same between I and I' . Otherwise, if they are not on the color discontinuity, they should be both specular pixels. The ambiguity between specular and color discontinuity is suppressed via the color discontinuity detection described in Equation (14).

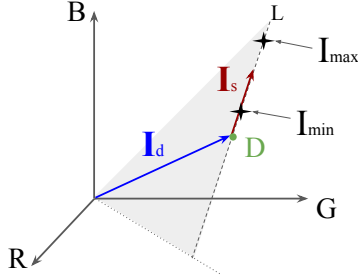


Figure 3: Diffuse I_d and specular I_s components in RGB space

335 *4.4.2. Specularity reduction*

The aim of this step is to find the specular part and the diffuse part of the so-called specular pixels, obtained from the preceding step. The main idea, based on Nayar et al. [3], is to assume that neighboring pixels have the same diffuse part. Thus the (known) diffuse part of the diffuse-only pixels (computed
340 in Section 4.3.1) will be used to assess the diffusion part of the specular pixels.

Let us recall that a specular pixel intensity is the sum of a diffuse component (I_d) and a specular component (I_s), and that it lies on a line defined by I_{min} and I_{max} . This line is the color constrain that can be obtained only through polarization. The line L is determined using the I_{max} and I_{min} found through
345 Equation (1). Since only the specular component I_s is polarized [14], by rotating the polarizer, $I(x)$ varies along the line L .

The process starts with specular pixels which are located at the edges of the specular region; for all of these pixels x_i belonging to the borders, its diffuse parts is computed as the mean of the diffuse part of their diffuse-only neighbors
350 y_j .

Note that not all neighboring pixels are used, only those which are close enough to the plane defined by the origin of the RGB space and L in Fig. 3, by checking if the angle between $I(y_j)$ and this gray plane is inferior to a threshold. The process is repeated iteratively. During the process, the components of
355 diffuse only pixels are used, or the diffuse component of pixels for which has just been computed, until all specular pixels have been processed. The end of

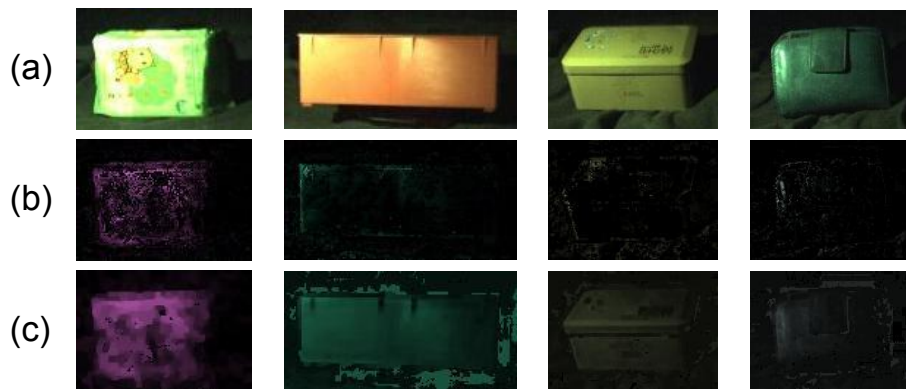


Figure 4: (a) Original image; (b) First approximate solution P_{init} ; (c) Final solution P by the proposed method

the process yields the $p_{init}(x)$ map, the first approximate solution, equal to 0 for diffuse-only pixels and to a non zero value for specular pixels.

5. Experimentation

360 5.1. Implementation and data

In the experiments, we compare the proposed approach to two well-known methods in the literature: Nayar’s method [3] which provides the state-of-the-art local specular and diffuse separation using polarization; Umeyama’s method which is a global polarization-based algorithm. The algorithm is implemented
 365 on Matlab 2012a and a C++ platform, and the energy function is solved through graph cuts with 4-connected neighbors using the gco_v3.0 library [18, 28, 29]. The problem of optimizing $p(x)$ is formulated as a global labeling problem, with labels ranging from 0 to 255. Regarding hyperparameters, it is worth to note that the specularity removal results are stable for λ_1 in the range [3.5, 7] and
 370 for λ_2 in the range [1.3, 1.7], regardless of the processed image. In the following experiments, hyperparameters are $\lambda_1 = 5$ (in Equation (6)) and $\lambda_2 = 1.5$ (in Equation (7)).

As far as we know, there is no public polarization-based benchmark. The proposed approach is evaluated on six images acquired with a polarization de-

375 vice composed by a polarizer² and a CCD camera³. In order to foster fair
bench-marking of specular removal methods on common data, we have made
our images available⁴.

5.2. Visual evaluation

In order to visually assess the specular part, we show four groups of images
380 (Fig. 4 (a)) with their first approximate solution P_{init} (Fig. 4 (b)) and their
final solution P (Fig. 4 (c)) given by our global method.

Let us now visually assess the specular removal on the diffuse component.
We show the results of six groups of images (Fig. 5 (a)) with four methods,
Umeyama’s method [16] (Fig. 5 (b)), Nayar’s method [3] (Fig. 5 (c)), our first
385 approximate solution (Fig. 5 (d)) and the proposed final solution (Fig. 5 (e)).
Umeyama’s method removes only a small part of the specular component, with a
reduction on the contrast. The reason is that the assumption of uniform incident
angle made by Umeyama does not hold on real images. It also proves that the
independency assumption alone is not able to yield a good result. The first ap-
390 proximate solution that we computed shows obvious improvement. Results are
similar but slightly better than Nayar’s, where we can see that the specularity is
only partially removed. Interesting to note is that the significant gain originates
from the first approximation. Since it is easy to compute, this approximation
may show promise for real-time operation. In order to further increase accuracy,
395 the global method leverages the independency assumption and the constraint
given by the first approximate solution, so as to handle the remaining noise,
and detect and remove more completely the specular component.

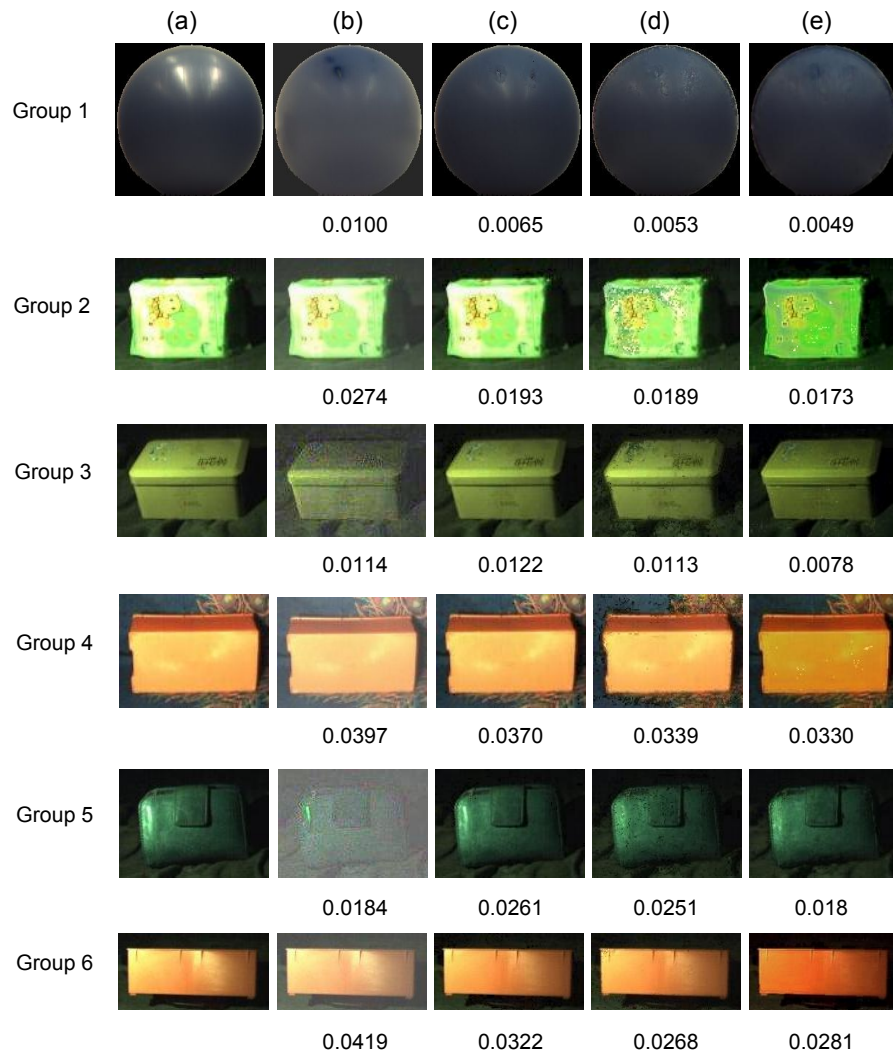


Figure 5: (a) Original image; (b) Results of Umeyama's method; (c) Results of Nayar's method; (d) First approximate solutions; (e) Results of the proposed method. The SD is given for each result image. Figure best viewed in color.

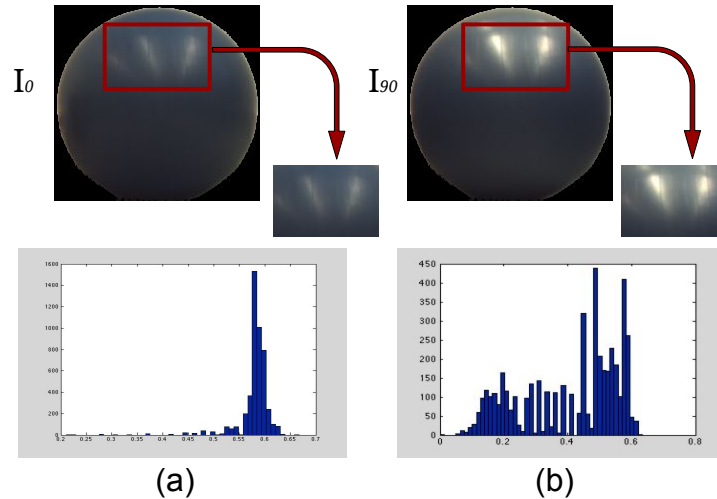


Figure 6: Histogram of hue values with (a) I_0 , weak specular reflection; (b) I_{90} , strong specular reflection

5.3. Quantitative evaluation

In the literature, only visual comparison of results from different methods
 400 is usually given, without any quantitative evaluation [13, 3, 30]. The reason is
 that, first, a ground truth is not always accessible; Second, the ground truth
 is usually acquired under an extreme dark illumination and thus not usable for
 error computation.

However we propose to evaluate the specular removal results using the
 405 Standard Deviation (SD) of the histogram distribution. Let us illustrate this
 criterion on an object with uniform color (hue) in Fig. 6. I_0 is acquired with a
 polarizer positioned at 0° and I_{90} at 90° . These images are analyzed in the HSV
 space, since the chromaticity is straightforwardly presented as hue in this color
 space. The histogram of hue values with weak specular reflections (Fig. 6 (a))

²<http://www.edmundoptics.fr/optomechanics/optical-mounts/polarizer-prism-mounts/rotary-optic-mount/1978/>

³http://www.theimagingsource.com/en_US/products/cameras/gige-cmos-ccd-color/dfk33gv024/

⁴<http://pagesperso.litislab.fr/fwang/fichiers/>

410 is more concentrated than the one with strong specular reflections (Fig. 6 (b)).
Standard deviation of hue values can thus be used to quantize the quality of
specularity removal: the smaller the SD is, the better the specular component
is removed. Note that this criterion is applicable only for images where the
specular reflection does not cover the majority of the image, and where the
415 texture of the original image is relatively simple.

The SD is computed for each resulting image in Fig. 5. It can be noted
that our proposed method also produce the best results as already observed
qualitatively, followed by the first approximate solution and Nayar’s method
[3]. Umeyama’s method [16] always produces the largest SD, except on group
420 5, which is hampered by a large whitening effect leading to a relatively small
SD value. However, when taking into account both the visual and quantitative
evaluations, we can conclude that our method still produces the best specularity
removal results on this set of images.

However room for improvement is left regarding the computation time. In-
425 deed, for a 240×320 pixel image, the execution time of the specularity removal
takes approximately 1.5 second for Umeyama’s method, 7 seconds for Nayar’s
method, and 10 seconds for the proposed method, including computing the first
approximate solution, data term and the optimization process, all measured on
a laptop running with a 2.6 GHz processor and 8GB RAM.

430 5.4. Robustness analysis

Local-based methods are usually based on the DOP. Since the DOP is com-
puted from at least three images, it is largely contaminated by noise. Local-
based methods are hence prone to suffer from noise. This motivates us to analyze
the performance of our method with respect to different noise levels.

435 White Gaussian noise with zero mean and varying values of σ is added to I_0 ,
 I_{45} and I_{90} . The SD of each group of images are computed correspondingly. Let
 SD_0 be the SD of the result without noise, \overline{SD} is normalized as $\overline{SD} = SD/SD_0$.
It is straightforward that when \overline{SD} is near to 1, it means that SD is nearly equal
to SD_0 , and the result is not largely influenced by noise. The mean (red point)

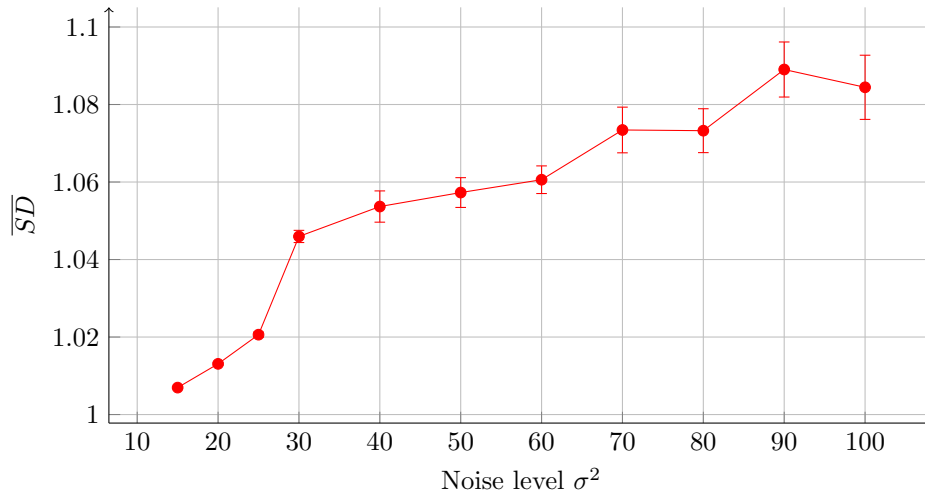


Figure 7: Quality of image with removed specularity w.r.t. added Gaussian noise: Mean \overline{SD} over the 6 images vs noise level σ^2 . The error bar refers to the variance of \overline{SD} over the 6 images.

440 and the variance (error bar) of \overline{SD} over the groups of Fig. 5 are computed and shown in Fig. 7.

For $\sigma^2 < 20$, little variation on \overline{SD} can be noticed. It can be seen that even by adding noise with $\sigma^2 = 25$, which is considerable, \overline{SD} still remains close to 1, and the change of SD is small, inferior to 5%. That is to say, our method
 445 remains stable against noise with $\sigma^2 \leq 25$. Note that noise with $\sigma^2 > 25$ rarely appears in real application thanks to improved camera quality. This experiment gives us some insight about the encouraging behavior of our method regarding robustness.

6. Discussion and future work

450 In this paper, we proposed a polarization-based global energy minimization approach to remove the specular component from images. This method is based on an independence assumption, with constraints given by a first approximate solution. Polarization information is used as a color constraint which largely reduces the color distortion produced by traditional color-based methods. The

455 robustness analysis also shows that the proposed method is stable for camera noise, which is quite problematic for classical local methods.

Regarding the data term of the global energy function, as a tradeoff between maximizing $\phi(p(x))$ while minimizing $D(p(s))$ is to be found, it has been simply and intuitively defined as the sum of a positive term and a negative term. 460 Alternatives include maximizing $\phi(p(x))/D(p(s))$ or the log difference. Future study may focus on a way to improve the design of the data term. To further improve the effectiveness of the smoothness term, we may want to consider to combine the $\Psi(\cdot)$ (Equation (6)) with the local intensity or the gradient of the intensity, as future work. In this way, the object boundary may be better 465 preserved.

The chromaticity information is essential in finding the first approximate solution, since the latter one is largely dependent on the variation of the chromaticity in terms of the specular component. If the specular component and the object shares the same chromaticity, we face the so-called blank wall problem, 470 as in stereo imaging, and the first approximate solution may be imprecise, since no optimum D can be found (as in Figure (3)).

As all specular removal methods, this method is designed to handle specular component which varies inside the camera sensor range $[0 - 255]$. If one of the color channels falls outside this range, the chromaticity information is permanently lost. In this case, the diffuse component of pixels which have lost their 475 chromaticity information is hardly recovered by specular removal method. In this case, inpainting methods, which are based on the smoothness assumption of texture, color, or other features [31], could for example be used.

The proposed method also extends the condition of single light source from 480 Umeyama et al. [16] to non-overlapping multi-sources. However, once the different light sources produce overlapping specular regions, the specular reflection on these pixels will be the mixed polarization pattern of two different sources, which can not be described using three parameters anymore. Possible solution for this problem might be to increase the numbers of captured polarization 485 images to infer the mixed polarization pattern. Regarding the handling of over-

lapping sources, one could be investigate the related field of time of flight cameras, where solutions for removing multipath interferences have been proposed [32, 33, 34].

Simulation of polarization images holds a lot of potential, especially regarding the reflection with different material and complex surface structure, in order to give a better way to evaluate the specular removal results or even more polarization-related algorithms. At last, we are currently engaged in adapting the separation scheme for outdoor images, especially road scene where the specular highlight can be problematic. In this regard, we aim at improving the execution time of our method, in order to reach real-time computation, an important issue in road scene image processing.

Acknowledgements

The authors would like to thank Carole Le Guyader for fruitful discussions and suggestions. The anonymous reviewers are also acknowledged for their detailed, qualified, and constructive reviews.

References

- [1] S. A. Shafer, Using color to separate reflection components, *Color Research & Application* 10 (4) (1985) 210–218.
- [2] O. Morel, F. Meriaudeau, C. Stolz, P. Gorria, Polarization imaging applied to 3d reconstruction of specular metallic surfaces, in: *Electronic Imaging 2005*, International Society for Optics and Photonics, 2005, pp. 178–186.
- [3] S. K. Nayar, X.-S. Fang, T. Boult, Separation of reflection components using color and polarization, *International Journal of Computer Vision* 21 (3) (1997) 163–186.
- [4] A. Hosni, M. Bleyer, M. Gelautz, Secrets of adaptive support weight techniques for local stereo matching, *Computer Vision and Image Understanding* 117 (6) (2013) 620–632.

- [5] M. Godec, P. M. Roth, H. Bischof, Hough-based tracking of non-rigid objects, *Computer Vision and Image Understanding* 117 (10) (2013) 1245–1256.
- [6] A. Artusi, F. Banterle, D. Chetverikov, A survey of specular removal methods, *Computer Graphics Forum* 30 (8) (2011) 2208–2230.
- [7] S. K. Nayar, G. Krishnan, M. D. Grossberg, R. Raskar, Fast separation of direct and global components of a scene using high frequency illumination, *Acm Transactions on Graphics* 25 (25) (2006) 935–944.
- [8] M. O’Toole, J. Mather, K. N. Kutulakos, 3d shape and indirect appearance by structured light transport, *IEEE Transactions on Pattern Analysis and Machine Intelligence* (2016) 1298–1312.
- [9] J. Kim, S. Izadi, A. Ghosh, Single-shot Layered Reflectance Separation Using a Polarized Light Field Camera, in: E. Eisemann, E. Fiume (Eds.), *Eurographics Symposium on Rendering - Experimental Ideas and Implementations*, 2016.
- [10] R. Tan, K. Nishino, K. Ikeuchi, Separating reflection components based on chromaticity and noise analysis, *Pattern Analysis and Machine Intelligence, IEEE Transactions on* 26 (10) (2004) 1373–1379. doi:10.1109/TPAMI.2004.90.
- [11] J. Yang, L. Liu, S. Li, Separating specular and diffuse reflection components in the hsi color space, in: *Computer Vision Workshops (ICCVW), 2013 IEEE International Conference on*, 2013, pp. 891–898.
- [12] H. Kim, H. Jin, S. Hadap, I. Kweon, Specular reflection separation using dark channel prior, in: *Proceedings of the IEEE Conference on Computer Vision and Pattern Recognition*, 2013, pp. 1460–1467.
- [13] R. T. Tan, K. Ikeuchi, Separating reflection components of textured surfaces using a single image, *Pattern Analysis and Machine Intelligence, IEEE Transactions on* 27 (2) (2005) 178–193.

- [14] L. B. Wolff, T. E. Boulton, Constraining object features using a polarization reflectance model, *IEEE Transactions on Pattern Analysis & Machine Intelligence* (7) (1991) 635–657.
- [15] M. Born, E. Wolf, Principles of optics: electromagnetic theory of propagation, interference and diffraction of light, Cambridge university press, 1999.
- [16] S. Umeyama, G. Godin, Separation of diffuse and specular components of surface reflection by use of polarization and statistical analysis of images, *Pattern Analysis and Machine Intelligence, IEEE Transactions on* 26 (5) (2004) 639–647.
- [17] A. Hyvärinen, J. Karhunen, E. Oja, Independent component analysis, Vol. 46, John Wiley & Sons, 2004.
- [18] Y. Boykov, O. Veksler, R. Zabih, Fast approximate energy minimization via graph cuts, *Pattern Analysis and Machine Intelligence, IEEE Transactions on* 23 (11) (2001) 1222–1239.
- [19] F. Wang, S. Ainouz, C. Petitjean, A. Bensrhair, Polarization-based specular removal method with global energy minimization, in: Proceedings of the IEEE International conference on image processing, 2016.
- [20] S. Ainouz, O. Morel, D. Fofi, S. Mosaddegh, A. Bensrhair, Adaptive processing of catadioptric images using polarization imaging: towards a polar-catadioptric model, *Optical Engineering* 52 (3) (2013) 037001–037001.
- [21] M. Saito, Y. Sato, K. Ikeuchi, H. Kashiwagi, Measurement of surface orientations of transparent objects using polarization in highlight, *Systems and Computers in Japan* 32 (5) (2001) 64–71.
- [22] Fluxdata, Imaging polarimeters fd-1655-p, <http://www.fluxdata.com/imaging-polarimeters>.

- [23] G. J. Klinker, S. A. Shafer, T. Kanade, The measurement of highlights in color images, *International Journal of Computer Vision* 2 (1) (1988) 7–32.
- [24] P. Z. Peebles, J. Read, P. Read, Probability, random variables, and random signal principles, Vol. 3, McGraw-Hill New York, 2001.
- 570 [25] V. Kolmogorov, R. Zabih, Computing Visual Correspondence with Occlusions using Graph Cuts, *IEEE*, 2001.
- [26] A. Miron, S. Ainouz, A. Rogozan, A. Bensrhair, A robust cost function for stereo matching of road scenes, *Pattern Recognition Letters* 38 (2014) 70–77.
- 575 [27] R. Zabih, J. Woodfill, Non-parametric local transforms for computing visual correspondence, in: *Computer VisionECCV'94*, Springer, 1994, pp. 151–158.
- [28] V. Kolmogorov, R. Zabih, What energy functions can be minimized via graph cuts?, *Pattern Analysis and Machine Intelligence, IEEE Transactions on* 26 (2) (2004) 147–159.
- 580 [29] Y. Boykov, V. Kolmogorov, An experimental comparison of min-cut/max-flow algorithms for energy minimization in vision, *Pattern Analysis and Machine Intelligence, IEEE Transactions on* 26 (9) (2004) 1124–1137.
- 585 [30] J. Yang, Z. Cai, L. Wen, Z. Lei, G. Guo, S. Z. Li, A new projection space for separation of specular-diffuse reflection components in color images, in: *Proceedings of the 11th Asian Conference on Computer Vision - Volume Part IV, ACCV'12*, Springer-Verlag, Berlin, Heidelberg, 2012, pp. 418–429.
- [31] M. Daisy, D. Tschumperlé, O. Lézoray, A fast spatial patch blending algorithm for artefact reduction in pattern-based image inpainting, in: *SIGGRAPH Asia 2013 Technical Briefs*, ACM, 2013, p. 8.
- 590 [32] J. P. Godbaz, M. J. Cree, A. A. Dorrington, Understanding and ameliorating non-linear phase and amplitude responses in amcw lidar, *Remote Sensing* 4 (1) (2011) 21–42.

- 595 [33] A. Bhandari, M. Feigin, S. Izadi, C. Rhemann, Resolving multipath interference in kinect: An inverse problem approach, in: *Sensors*, 2014, pp. 614–617.
- [34] D. Freedman, Y. Smolin, E. Krupka, I. Leichter, M. Schmidt, *SRA: Fast Removal of General Multipath for ToF Sensors*, Springer International Publishing, 2014.
- 600